Available online at www.sciencedirect.com
SCIENCE DIRECT®
Polymer 44 (2003) 6913–6925
polymer
www.elsevier.com/locate/polymer

Amplification effect of platelet type nanoparticles on the orientation behavior of injection molded nylon 6 composites

B. Yalcin, D. Valladares, M. Cakmak*

Institute of Polymer Engineering, Department of Polymer Engineering, University of Akron, Akron, OH 44325-0301, USA

Received 23 April 2003; received in revised form 17 July 2003; accepted 29 July 2003

Abstract

The effect of platelet type nanoparticles and processing conditions; mold temperature and injection speed, on the development of local microstructure in injection molded nylon 6 parts was investigated. The molded parts exhibit two crystal forms (α and γ) of nylon 6 in varying proportions from skin to core. The γ crystals preferentially grow near the surface regions and α crystal fraction increases with distance from the surface in all molded parts. However, the spatial variation of crystal phases across the thickness in nanocomposites differs from that of unfilled nylon 6. Nanoplatelets induce high levels of orientation of the polymer matrix throughout the thickness of the molded part even at high mold temperatures where nonisothermal effects are highly suppressed and confined to very close proximity of surfaces. These high chain orientation levels observed in nanoparticle filled systems is a result of the shear amplification effect that occurs in small spaces between adjacent nanoparticles of differing velocity. The local preferential crystalline orientation of nylon 6 resin and nanoparticles across the thickness of the molded parts are investigated using a series of structure characterization techniques including microbeam wide angle X-ray, SAXS and TEM.

Keywords: Injection molding; Orientation; Nanoplatelet-fillers

1. Introduction

The particulate fillers of various type and shape have been utilized in polymers to produce composite materials with improved properties while reducing their cost [1]. Platelet type nanofillers in particular have received special recognition in the last decade due to their distinct property improvements at low loadings. This is due to substantially enhanced interaction between the polymer and single layers of these nanosilicate fillers with high surface area and aspect ratio [2].

Nylon 6 nanocomposites, pioneered by Toyota researchers have been extensively studied [3–12] for their preparation techniques and final properties. There have also been a few attempts made to understand the influence of processing conditions on the structural evolution and resulting properties in nylon 6 and its nanocomposites [13–15]. However, the effect of [16–21] spatio-temporally varying thermal-deformation fields experienced during injection molding on the complex structural gradients along and across the flow in injection molded parts have not been elucidated in these systems.

In this study, our purpose is to determine the effect of nanoparticles and processing conditions on the local structural hierarchy of nylon 6 developed under thermal and deformation fields experienced in injection molding process. The main focus is on the microstructure defined by the local preferential crystalline orientation of nylon 6 resin and nanoparticles across the thickness of the molded parts.

2. Experimental

2.1. Materials

Nylon 6 general-purpose homopolymer resin (Capron® 8202) and experimental nylon 6 packaging grade nanocomposite resin (Capron® XA-2744) with a density of 1.13 g/cm^3 were kindly provided in the form of pellets by Allied Signal Honeywell Corporation. Capron® XA-2744 was prepared at a loading of 5%-wt by melt compounding in

* Corresponding author. Tel.: +1-330-972-6865; fax: +1-330-258-2339.
E-mail address: cakmak@uakron.edu (M. Cakmak).

0032-3861/$ - see front matter © 2003 Elsevier Ltd. All rights reserved.
doi:10.1016/j.polymer.2003.07.010

a twin-screw extruder. The viscosity of unfilled nylon 6 and nylon 6 nanocomposite was measured at 250 °C using an Instron capillary rheometer.

2.2. Sample preparation

The samples were injection molded with a Van Dorn (Model HP with a Pathfinder 1000 controller) 55 Ton reciprocating-screw injection-molding machine equipped with a standard ASTM test mold and an oil circulating mold temperature controller. The samples with a thickness of 3 mm were prepared at two different mold temperatures (50, 130 °C) and injection speeds (2.02, 17 cm/s). The rest of the processing variables including melt temperature (250 °C), injection pressure (4481620 Pa), screw rotation speed (100 rpm) and clamp closed time (1 min holding followed by cooling) was kept constant. Large end-gated injection molded tensile bars were chosen for all the analysis.

2.3. Sample cutting procedure

Due to the existence of two mirror symmetry planes in a typical end-gate dumbbell shape molded bar, one in flow direction–transverse direction (FD–TD) and the other in flow direction–normal direction (FD–ND) plane, the characterization process is undertaken on the one-fourth unique quadrant of the sample bar. These directions and planes are shown in Fig. 1.

Each structural analysis technique required different cutting tools, procedures and thickness values suitable for investigation. The cutting tool, procedure and thickness values for each analysis technique are indicated in Table 1. Two cutting procedures employed for X-ray analysis were A-cut and B-cut procedures. In procedure A the samples were sectioned perpendicular to the flow direction in the (TD–ND) plane whereas in procedure B the samples were cut parallel to the flow direction in the (FD–ND) plane. These procedures are also shown in Fig. 1.

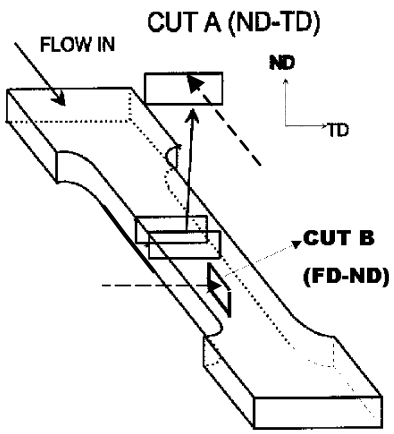

Fig. 1. Sample cutting procedures A, B.

2.4. Microbeam WAXD

Microbeam WAXD film patterns of unfilled nylon 6 and nanocomposite samples were taken at a series of locations from skin to core in the FD–ND plane with X-ray beam directed along the transverse direction using the matrixing microbeam X-ray camera (MMBX) developed in our laboratory [16]. The camera was mounted on a 12 kW Rigaku rotating anode generator operated at 40 kV and 150 mA. A 50 μm diameter Cu Kα beam obtained using a nickel foil monochromator and a pinhole collimator allowed highly localized skin to core (1500 μm) mapping of the B-cut samples with a precision *x-y* translation stage.

WAXD film patterns obtained was first captured and then digitized along the azimuthal direction for quantitative measurements using a 16-bit CCD camera software (photometrics-cooled CCD) operated by IPLab spectrum software. However, the presence of two different crystal structures (α and γ) and bimodal orientation taking place in certain local regions along the thickness of the nanocomposite samples results in rather complex orientation calculations. Therefore, uniaxial orientation calculations for the *a*, *b* and *c* crystallographic axes was only performed in the core regions of samples molded at 50 since fiber symmetry exists only in this region within the probing range of the 50 μm X-ray beam. This assumption was also in accordance with the observed film patterns of the core region of these samples.

The orientation functions were determined for the monoclinic α and γ forms of nylon 6 separately. Monoclinic α form has two strong reflections (200) and (002 + 202) doublet. Monoclinic γ form has one reflection from triplet $(001 + 200 + 20\bar{1})$. The orientation of the *a*, *b* and *c* crystallographic axes were determined with respect to the local symmetry axis which may not be necessarily along the flow direction. For this purpose, azimuthal intensity profiles of α monoclinic (002 + 202) and γ monoclinic $(001 + 200 + 20\bar{1})$ were used. It should also be kept in mind that the orientation function of the crystalline chains for the case of nylon 6 corresponds to f_b. The orientation functions were determined using Wilchinsky's geometrical rule [22] for the monoclinic α and γ form. The equations are presented in Appendix A.

The relative amounts of the α and γ crystal forms were determined from skin to core using the area under the plot of azimuthal intensity profiles of the corresponding planes of each crystal form. The following relationship was then used to obtain the relative amounts of α and γ forms of nylon 6 crystals.

$$\gamma/\alpha = [A_{\gamma(001+200+20\bar{1})}]/[A_{\alpha(200)} + A_{\alpha(002+202)}] \quad (2.1)$$

where *A* stands for area.

Table 1
The cutting tools, procedure and thickness values for the structural analysis techniques employed in the research

Analysis technique	Cutting tool	Cutting procedure	Section thickness (μm)
WAXD, SAXS	Leco Varicut VC-50 Diamond saw	A-cut, B-cut	300
Optical microscopy	Reichert-Jung 2050 microtome	B-cut	20
TEM	Reichert-FCL Ultra microtome	B-cut	0.05

2.5. Optical microscopy

In order to show the physical locations where the WAXD patterns were obtained, the polarized light microscopy images of B-cut samples were taken. Samples were placed on a Leitz Laborlux 12 Pol S microscope stage oriented with their long axes (FD) at 45° to polarization directions of crossed polarizers. The pictures of the samples were taken with a Sony 3-chip 8-bit CCD camera connected to a color video printer.

2.6. SAXS

SAXS studies on injection molded nylon 6 samples were performed on a GE X-ray generator operated at 30 kV and 30 mA equipped with a Furnace X-ray camera. Nickel foil filter was used to obtain Cu Kα radiation and vacuum was applied to the camera to reduce the air scattering. The sample to film distance was 42.4 cm. SAXS experiments were performed on samples sectioned using A-cut and B-cut procedure at three regions across the thickness using a 500 μm diameter pinhole. For B-cut samples the X-ray was directed along the TD direction and was perpendicular to the FD–ND plane of the sample whereas for A-cut samples the X-ray was in the FD direction being perpendicular to the ND–TD plane of the sample.

SAXS experiments with sample rotation about the flow direction were also performed. The methodology of this experiment is shown in Fig. 2.

2.7. Transmission electron microscopy

Transmission electron image was obtained using a JEOL 1200EX microscope with an accelerating voltage of 80 kV. Sample was taken from the FD–ND plane close to the skin region using an ultra microtome. Since SAXS measurements are more reliable than any given electron microscope observation, the overall picture of the distribution and dispersion of nanoplatelets across the entire thickness of the sample was mainly constructed using SAXS. However, the micrograph was needed at least at one point to visualize the origin of the nature of the scattering pattern seen in SAXS. Fig. 3 shows the sampling procedure.

3. Results and discussion

3.1. Preliminary studies

The viscosity data for unfilled nylon 6 and nylon 6 nanocomposite are shown in Fig. 4. Nylon 6 nanocomposite exhibits higher viscosity values than that of unfilled nylon 6 at 250 °C that is also the temperature chosen for injection molding. The extrapolation of the curves to typical high shear rate values of $10^3\ s^{-1}$ encountered during processing predicts that the relative viscosities will remain similar.

In order to assess the crystal form development in the absence of shear, we also prepared compression molded samples at 250 °C and air-cooled to room temperature. Wide angle X-ray diffraction scans of compression-molded samples are shown in Fig. 5. Unfilled nylon 6 exhibits two intense α diffraction peaks at 20.5 and 24° corresponding to (200) and the (002), (202) doublet and one weak γ peak at 21.5° belonging to $(001 + 200 + 20\bar{1})$. Cooling the compression-molded part in air resulted in α form growth in nylon 6 that is typical of slow cooled samples. The γ form of nylon 6, on the other hand, is favored only when the nylon 6 melt experiences high degrees of supercooling accompanying fast cooling rates

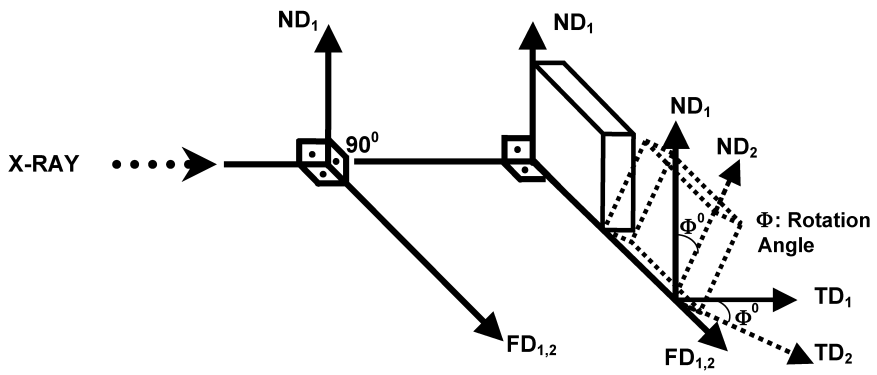

Fig. 2. SAXS method of experimentation with sample rotation.

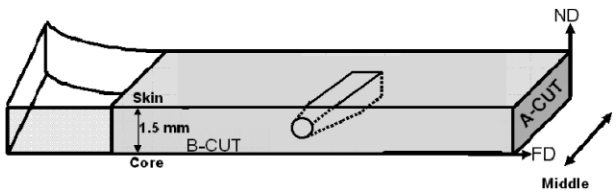

Fig. 3. TEM sample preparation procedure.

in the absence of flow [23]. When nanoparticles are incorporated, nylon 6 shows intense γ diffraction peak and traces of α peaks in the sample compression molded at 250 °C and air cooled that is considered slow cooling.

These combined results suggest that during crystallization in the absence of deformation, the nanoplatelets favor the formation of γ-crystallites, even under slow cooling conditions to room temperature that would normally favor α form of nylon 6 [11].

3.1.1. Level of nanoplatelet dispersion in received samples

The level of dispersion or exfoliation of silicate platelets in nanocomposite systems is usually determined by the nature of the X-ray diffraction peak around 5° 2θ that belongs to (001) planes of montmorillonite nanoplatelets. The shift of the peak to lower values is interpreted as the expansion of clay galleries due to polymer chain intercalation. In Fig. 5 nanocomposite sample has a low angle tail whose intensity increases with decreasing scattering angle. This indicates that we have substantial intercalation of the nanoparticles in the nanocomposite samples before injection molding. TEM results to be discussed below will show that there is ample evidence for substantial exfoliation of clay platelets in injection molded samples.

3.2. Local orientation and spatial distribution of crystalline phases

Microbeam WAXD mapping of B-cut samples along the thickness of the molded part was performed for unfilled nylon 6 and its nanocomposites. The optical images of the B-cut samples are presented here for the sole purpose of revealing the locations at which the WAXD patterns were taken. The detailed optical microscopy study is the subject of a companion paper [24].

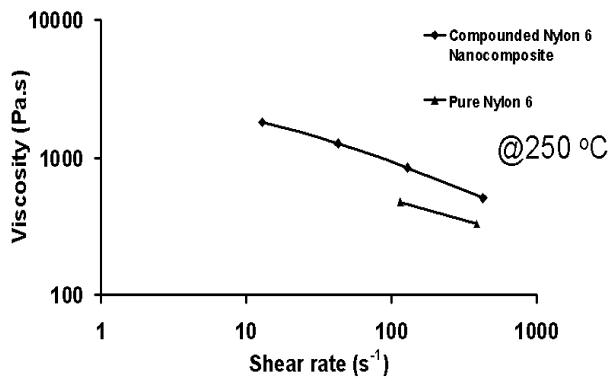

Fig. 4. Viscosity vs. shear rate for the unfilled and nanoparticle filled nylon 6.

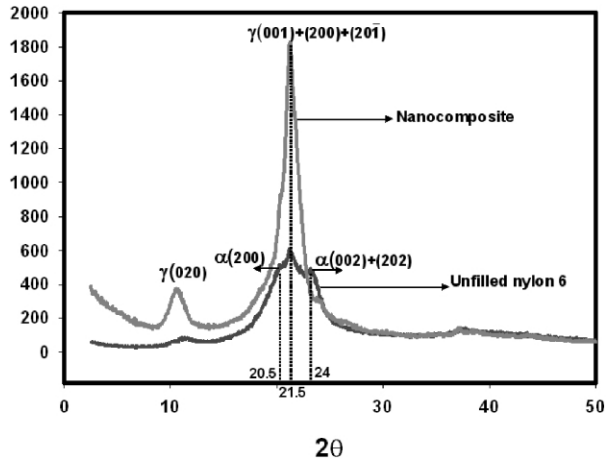

Fig. 5. X-ray diffraction scans of samples.

Typical WAXD patterns of α and γ crystal forms of nylon 6 are presented in Fig. 6 in order to help in interpretation from more complex WAXD patterns.

The α form of nylon 6 exhibits two strongly diffracting planes. The one appearing at higher angle (α_1) is a mixture of (002) and (202). The second one at lower angle (α_2) represents (200) plane that belong to currently accepted monoclinic form nylon-6 [25] with, $a = 9.56$ Å, $b = 17.24$ Å (chain axis), $c = 8.01$ Å, and $\beta = 67.5°$.

The γ form exhibits a single characteristic crystalline reflection that is composed of the merging of three diffraction spots (001), (200) and (20$\bar{1}$). The γ crystal form of nylon-6 was reported by Kinoshita [26] and Arimoto [27,28] along with many others [29–33]. This form of nylon-6 has the monoclinic structure with $a = 9.33$ Å, $b = 16.88$ Å (chain axis), $c = 4.78$ Å, and $\beta = 121°$ [27].

3.2.1. Unfilled nylon-6

Structural variation across the thickness as revealed by micro WAXD technique is shown in Fig. 7 for 50 and 130 °C mold temperatures. Among all of these WAXD patterns, the only one that shows preferential orientation is the surface region (0–50 μm) in the sample molded at 50 °C. It also exhibits asymmetry with the X-ray beam directed along the TD indicating that the local symmetry axes in this layer are tilted away from the FD–ND plane towards the core. All other locations and conditions show essentially unoriented WAXD pattern. Although nylon 6 is considered a fast crystallizing polymer, it does not show distinct layers of oriented structures as in the case of polypropylene at comparable temperatures [34]. This is primarily due to very low melt viscosities.

At 50 °C, 700 μm thick layer adjacent to the mold surface is exclusively in γ crystal form. Beyond this layer, the population of α crystals increases towards the core. This result is in accord with the published literature where the

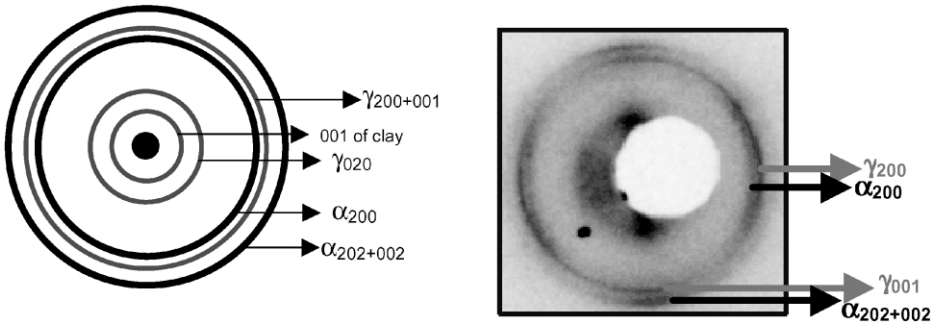

Fig. 6. Typical WAXD patterns of α and γ crystal forms of nylon 6.

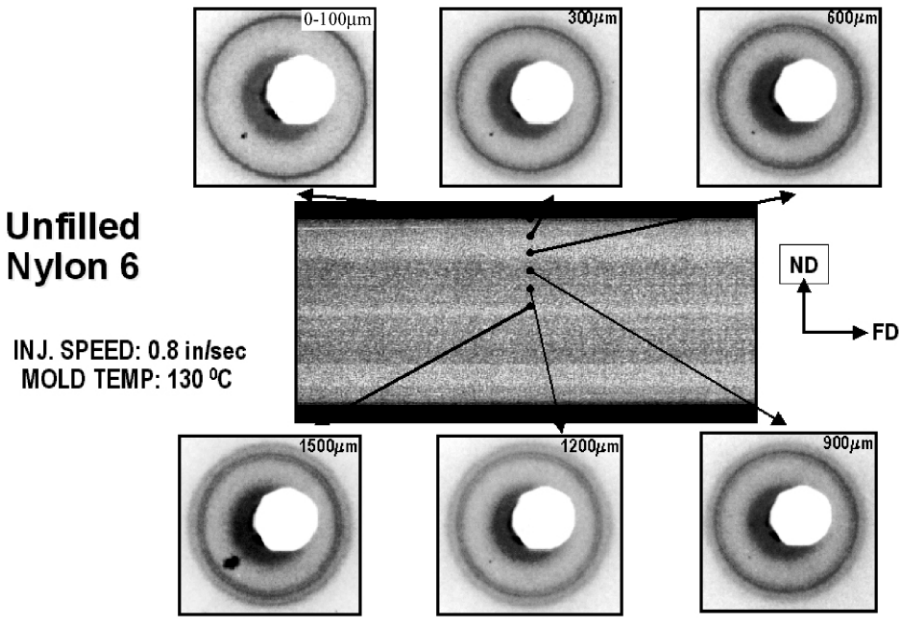

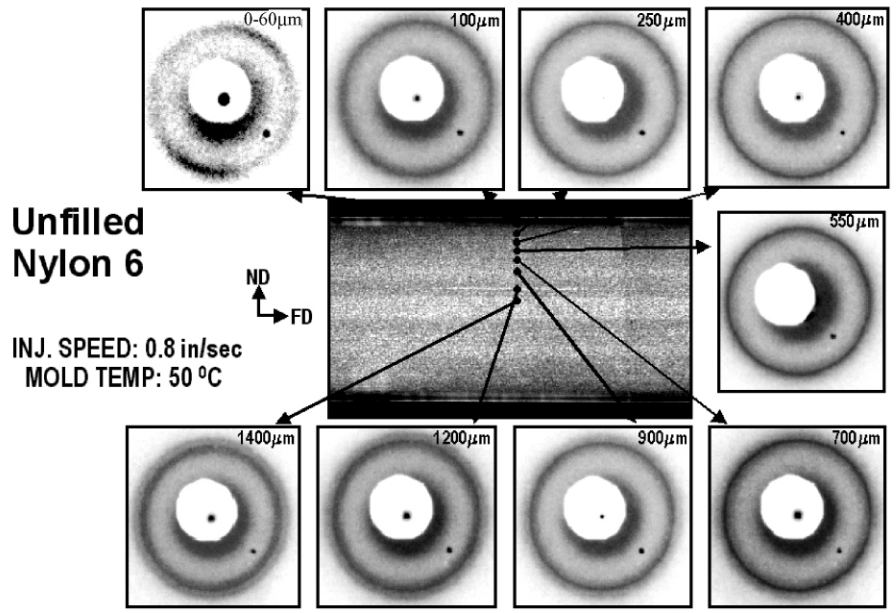

Fig. 7. Micro WAXD patterns obtained from skin to core.

reduction of cooling rate was shown to result in the formation of α form [23,35,36]. The γ form is known to grow under fast cooling conditions [23]. When the nylon 6 is molded at high mold temperature all the crystal formations throughout the part including the skin region experience substantially slower cooling with the slowest cooling rate experienced at the core. This, in turn, result in a thinner surface layer (300 μm) exhibiting exclusively γ form with the remaining core regions showing increasing fraction of the α crystal form. The relative proportion of the phases were determined and plotted in Fig. 8 for samples molded at 50 and 130 °C. As indicated earlier, both samples exhibit surface regions that are exclusively in α form. The α form first appears at 300 and 750 μm from surface for low and high mold temperatures, respectively. With increasing distance from the surface, γ/α ratio decreases reflecting the enrichment of core regions with α form crystals.

3.2.2. *Effect of nanoparticles*

The microbeam wide angle X-ray mapping of the nanocomposite samples is shown in Fig. 9 for both 50 and 130 °C mold temperatures. The WAXD patterns indicate that the surface layers are in γ form. As we have seen in unfilled nylon 6 there is a gradual increase of the α form towards the core. In fact, the distance at which the α form first appears in nanocomposite samples is the same as in unfilled samples for each mold temperature (compare Figs. 7 and 9). However, the spatial variation of crystal phases across the thickness in nanoparticle filled system differs from that of unfilled nylon 6.

For nanocomposites the spatial variation of crystal phases is governed not only by the temperature gradient experienced across the thickness but also by the nanoparticles, especially by the local deformation fields they impose on the nearby polymer chains. The mechanical shearing of unfilled nylon 6 was recently reported to induce α form under nonisothermal crystallization conditions [37]. On the other hand, in compression molded samples where the shear deformation is minimal, we have shown that the nanoparticles favor the formation of γ form of crystals (see Section 3.1) even when the sample is cooled slowly that would normally favor α form of crystal growth. Similarly, regular nucleating agents or macro fillers were shown to promote γ form of nylon 6 in compression molding and in injection molding [14].

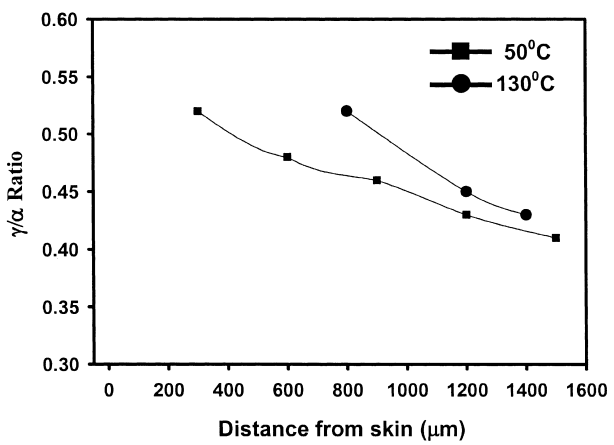

Fig. 8. Fraction of γ form of crystals from skin to core along FD–ND plane (mold temp: 50 °C and 130 °C, injection speed: 0.8 in/sec).

Nanoplatelets, on the other hand, promote preferential growth of α-form if we compare the phase behavior at 900 μm depth for unfilled and nanoparticle filled nylon 6 molded at 130 °C (see Figs. 7 and 9). In this region the WAXD pattern for the nanocomposite exhibits only α crystal planes while for unfilled nylon 6 major diffraction is from γ planes. Since the thermal effects are similar at the same depths, obviously the shear deformation is responsible for the growth of α form of nylon 6. The same is true for nylon 6 molded at 50 °C (compare WAXD at 900 μm distance). At low mold temperatures one would expect a more significant shear effect especially near the surface regions that should result in α-crystal formation. The fact that we observe the surface regions to be in γ form indicates that in this region the thermal effects associated with fast cooling rates [23] dominates over the flow effects [37].

A striking feature of the WAXD patterns for nanocomposites is that the nylon 6 crystallites are very highly oriented even in the core regions. This is surprising since at such high mold temperatures (130 °C) the shear effects due to sharp thermal gradients prevalent at low temperatures are significantly reduced.

In order to determine the orientation of samples with fiber symmetry, it is sufficient to take WAXD patterns in one direction, usually this being perpendicular to the drawing direction. The orientation of the crystal planes in injection-molded samples on the other hand requires more than one direction. This is especially true in cases where fiber symmetry does not apply at local level. The out of plane orientation of the main crystal chain axis, b^* of the reciprocal lattice, is seen in Fig. 9 in the intermediate regions. The b^* axis of the reciprocal space represented by the (020) plane is oriented in the flow direction in the top 250 μm layer as evidenced by the equatorial diffraction (see block arrow on WAXD pattern at 200 μm). Following this region, the diffraction from this plane disappears (see WAXD pattern at 450 μm) and once again appears in the core region on FD–ND plane in the normal direction with a slight tilt (see the tip of the block arrow at 1000 μm). The schematic presentation of the regions from skin to core is shown in Figs. 10 and 13. In Fig. 10 the presence of (020) and (001) planes on the WAXD patterns obtained from B-cut samples and the presence of (001) and (200) planes on the WAXD patterns obtained from A-cut samples indicates that close to the skin region, b^* and c^* axis of the reciprocal space is oriented in the flow and normal direction, respectively. The a^* axis is oriented out of the FD–ND plane. Four strong diffraction peaks at $\pm 60°$ and $\pm 120°$ azimuthal angles from (200) plane on the WAXD pattern of the A-cut sample also supports this observation. In Fig. 11

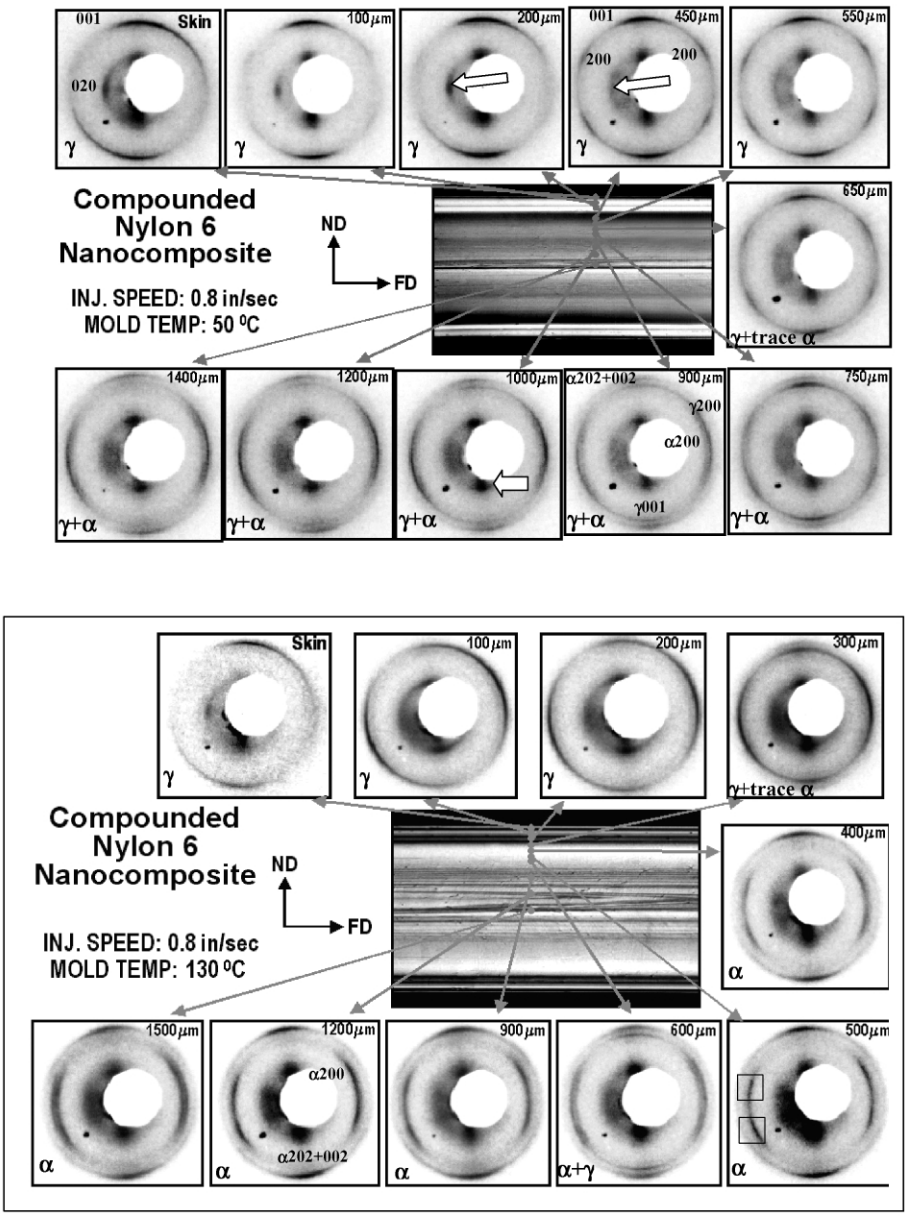

Fig. 9. Micro WAXD patterns obtained from skin to core.

the presence of four diffraction peaks at ±60° and ±120° from (200) peaks on the WAXD pattern of the A-cut and B-cut sample simultaneously indicates that the region 250–650 μm exhibits crisscross γ crystal forms. It should be noted that in this region it is the *a*-axis of the real space and not the reciprocal space that is oriented in the flow direction. This is in contrast to the 0–250 μm region where the *b*-axis (chain axis) of the real space is oriented in the flow direction. Following this region, the α-crystal form starts to appear along with the γ form and both forms assumes crisscross orientation with the *a*-axis of the real space still oriented in the flow direction. This is shown in Fig. 12. The region 750–1500 μm has rather complex nature since the occurrence of α crystal form is more apparent. This is shown in Fig. 13.

The most remarkable observation for samples molded at 130 °C is perhaps similarity of the diffraction patterns in the core regions to that of doubly oriented nylon 6 (see square marks in Fig. 9) films annealed at high temperatures possessing α form of crystal structures [38]. The diffraction patterns corresponding to region 400–1500 μm are almost similar with the γ and α crystals differing in their relative amounts. A quantitative idea of the orientation levels was obtained through Wilchinsky's geometrical rule for the core regions of the samples molded at 50 °C in Fig. 9 where uniaxial local symmetry is observed. The orientation function for the *b*-axis was calculated and found to be 0.6. Such high orientation levels in the core of the injection molded parts to our knowledge has not been observed before and attributed solely to the effect of nanoparticles.

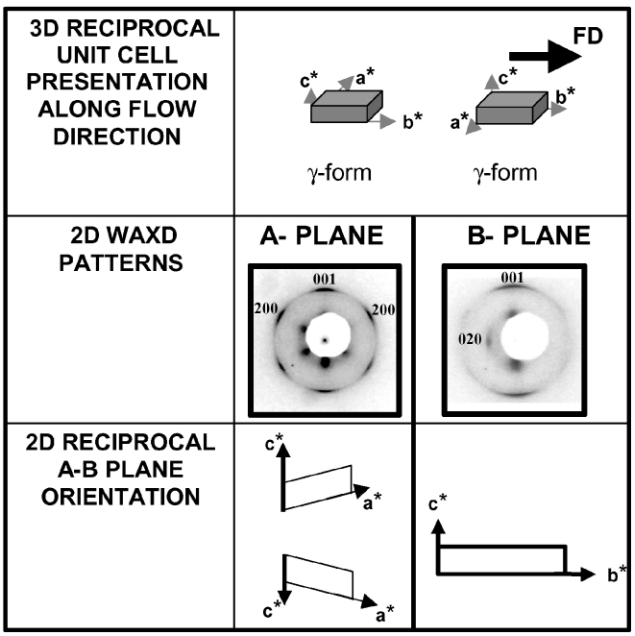

Fig. 10. Schematic representation of the crystal unit cell orientation close to skin region (0–250 μm) for melt compounded nano with 50 °C MT and 0.8 in/s IS.

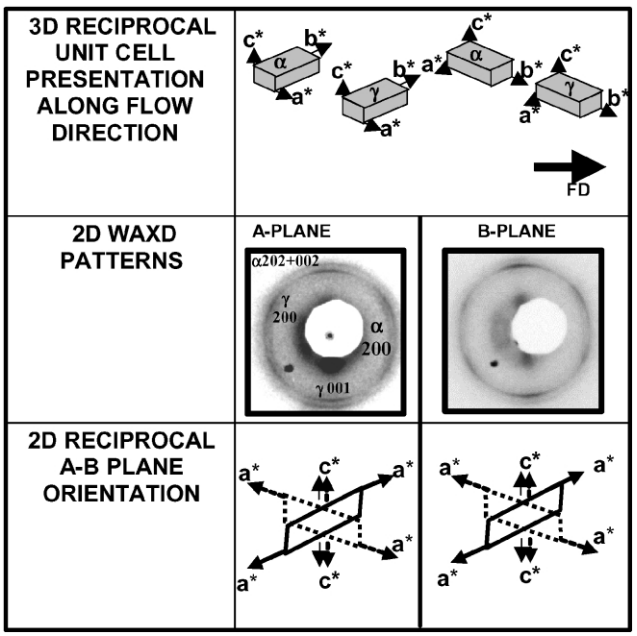

Fig. 12. Schematic representation of the crystal unit cell orientation close to skin region (650–750 μm) for melt compounded nano with 50 °C MT and 0.8 in/s IS.

3.3. Orientation of nanoplatelets as detected by SAXS and TEM

The orientation of the nanoplatelets was investigated by SAXS and TEM. Thin platelet nature of nanoparticles and their ability to orient in a shear field allows us to determine their organization in a flow field using SAXS.

SAXS patterns of the B-cut samples molded at 50 °C are shown for three different locations from skin to core in Fig. 14. X-ray beam was directed along the transverse direction normal to the FD–ND plane. The streak patterns in the normal direction indicate that in real space the nanoplatelets are oriented nearly parallel to one another in the FD–TD plane with a wide distribution of gap distance between them leading to broadening of the streak in scattering angle direction. This pattern tilts away from the FD and broadens

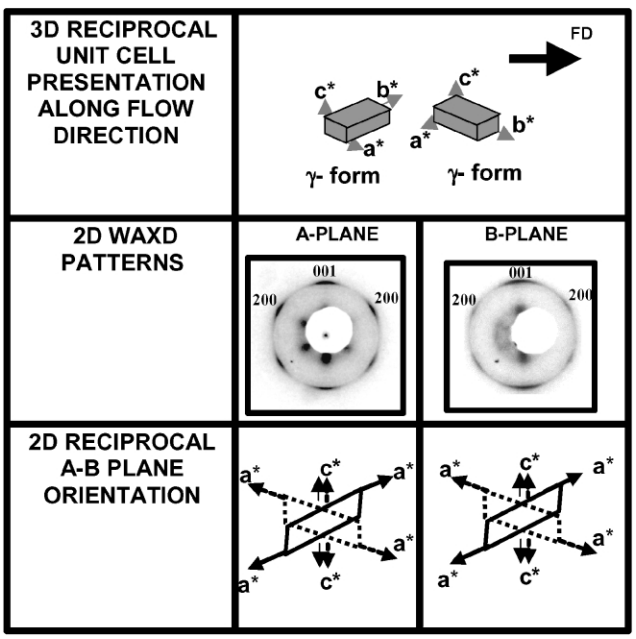

Fig. 11. Schematic representation of the crystal unit cell orientation close to skin region (250–650 μm) for melt compounded nano with 50 °C MT and 0.8 in/s IS.

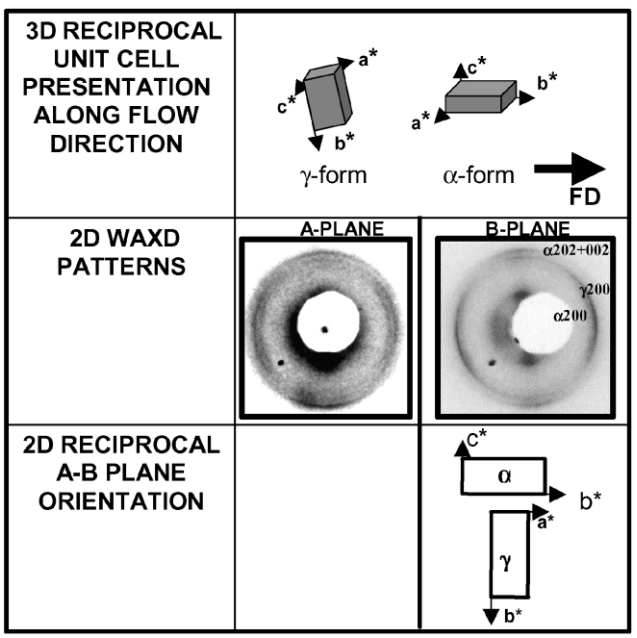

Fig. 13. Schematic representation of the crystal unit cell orientation close to skin region (750–1500 μm) for melt compounded nano with 50 °C MT and 0.8 in/s IS.

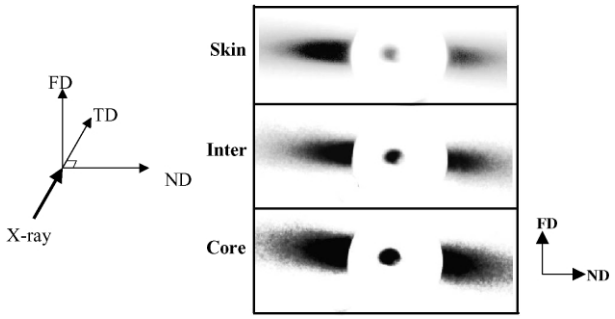

Fig. 14. SAXS patterns taken at three locations from skin to core of B-cut nanocomposite samples molded at 50 °C and 0.8 in/s. X-rays are directed along transverse direction and normal to the FD-ND plane of the sample (unrotated) (2 h exposure).

in azimuthal direction towards the core. This clearly illustrates that there is a cooperative reorientation of platelets and their parallelism with each other decreases towards the core as shown in Fig. 14. The normals of the nanoplatelets were found to be tilted inherently 2–6° from the normal direction of the sample. SAXS patterns of the A-cut samples along with that of the B-cut samples are shown in Fig. 15. Since the nanoplatelets are primarily oriented in FD–TD plane showing slight tilting towards FD direction, the streak patterns are still observable throughout the thickness direction on the A-cut samples. This is especially true for the skin and intermediate regions. The streak pattern of the core region, however, was not as apparent as that of the skin and intermediate regions. This is because the nanoplatelets in the core regions exhibit less parallelism with each other (increase of azimuthal spread of the streak) as compared to skin and intermediate regions. In addition these platelets tilt more towards the core. This substantially reduces the scattering in A-cut as the nanoparticle correlation is substantially reduced in this orientation thereby leading to suppression of SAXS scattering.

SAXS patterns obtained from samples molded at 130 °C is shown in Fig. 16. The streak patterns are still observable in the skin and intermediate regions for both the B and A-cut samples at this temperature. The streak pattern greatly reduces in the core regions. Concurrent reduction of the streak patterns on the B- and A-cut samples indicates that the orientation of the platelets in this region indicates the platelets are in near random state.

Another method of experimentation to support for the parallelism of the nanoplatelets is to take SAXS patterns at a series of rotation angles. If they are well aligned with each other there should be very small angular range where they would scatter. This is due to the fact that thickness of the nanoplatelets are in nanometer scale and other two dimensions are typically in micrometer of sub-micrometer scale and only correlations in the edge-on view falls within the detection range of SAXS. If there were a wider distribution, then this angular range in which scattering is observed would be larger. Fig. 2 illustrates this method of experimentation.

Fig. 17 shows that 20° of sample rotation about FD results in the disappearance of the streak pattern in the skin region of B-cut samples molded at 50 °C. This ensures that the platelets are almost parallel to the flow direction with normals of nanoplatelets oriented in the normal direction. Schematics of the orientation and organization of the nanoplatelets according to SAXS observations are shown in Figs. 18 and 19 for 50 and 130 °C mold temperatures, respectively.

A more direct visual investigation of nanoplatelet orientation was also carried out by TEM where the nanoplatelets are shown in Fig. 20 to be oriented in the flow direction. The origin of the streak scattering pattern seen in SAXS patterns is supported by the transmission electron microscope image. TEM image also illustrate the distribution of spacing between the layers. The nanoplatelets are organized 5–60 nm apart from each other.

3.4. Shear amplification mechanism

The development of shear zone close to the surface regions was reported for both injection-molded fast and slow crystallizing polymers [16–21]. For unfilled polymers two fronts established during injection molding are effective in the formation of the shear zone. One is the time varying front that defines the solid–liquid boundary that moves

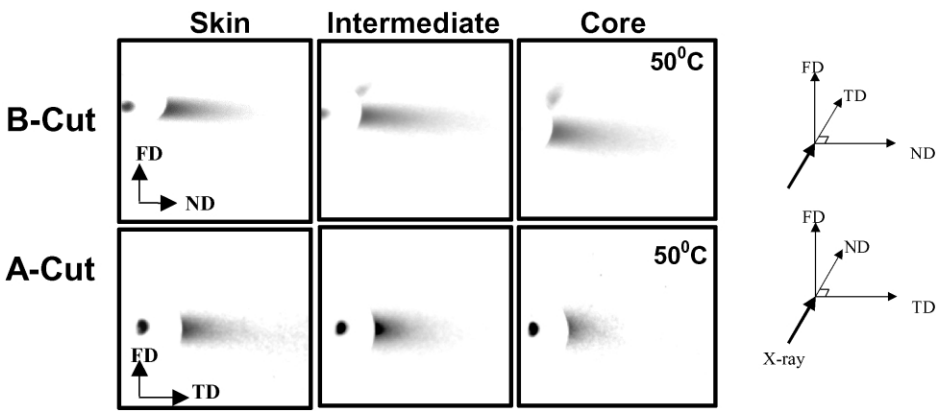

Fig. 15. SAXS patterns of unrotated B and A-cut nanocomposite samples molded at 50 °C (30 min exposure).

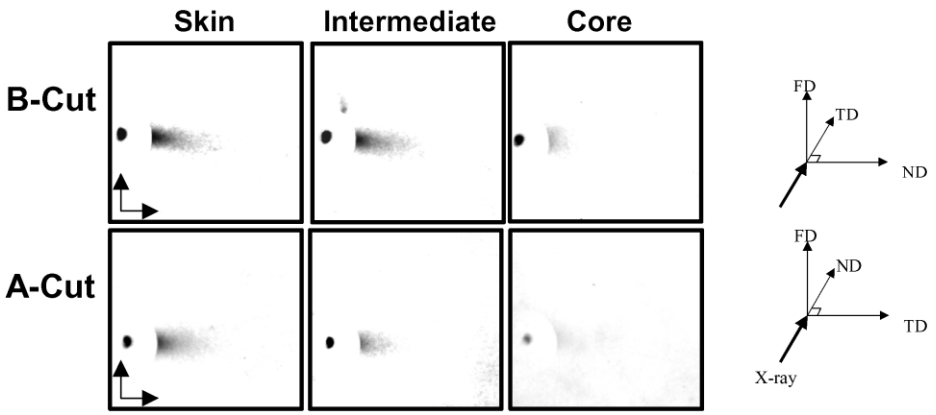

Fig. 16. SAXS patterns of unrotated B and A-cut nanocomposite samples molded at 130 °C (30 min exposure).

towards the interior of the part and the other one is the flow front. In injection molding of unfilled polymers, the chains experience shear deformation mainly due to the reduction in effective cross-sectional area of the melt zone as the solid–liquid boundary moves towards the interior of the part. The polymers caught in this regime are rotated, extended and finally frozen into their oriented morphologies.

When nanoplatelets are introduced into the flow field, the polymer chains experience significantly increased shear deformation within the narrow gaps of the platelets moving with different speeds. TEM evidenced that the nanoplatelets were 10–60 nm apart and SAXS studies corroborates this observation. The mechanism of shear amplification with reduction in gap distances is shown in Fig. 21.

A simple quantitative analysis of shear rate during mold filling process for an end-gated strip can be performed for unfilled nylon 6 by assuming an incompressible, isothermal and Newtonian fluid under fully developed flow. For filled nylon 6 an approximate shear rate can be calculated by considering the deformation of the polymer between two parallel infinite nanoplatelets moving with different velocities along with similar assumptions for the fluid properties. If we assume the upper nanoplatelet to be stationary relative to the other one, we can calculate the velocity profile along the normal direction and hence the shear rate using the momentum balance equations and a simple stress–strain relationship. The results show approximately 4000–40,000 times amplification in shear depending on the relative velocity assumed for lower nanoplatelet for the case of filled nylon 6. The equations and details of the analysis are presented in Appendix A.

4. Conclusions

In the small gaps between the nanoplatelets, the polymer chains experience ‘shear amplification effect’ during flow in injection molding. This leads to substantial orientation of polymer chains throughout the molded parts. The presence of nanoparticles desensitizes the developed structure to the changes in the processing conditions essentially widening the optimum processing window. Based on our results anisotropic nanoparticles could be used as orientation enhancers for the polymers during injection molding process once the compatibility and dispersion issues are solved. This behavior is very similar to those observed in thermotropic liquid crystalline polymers [39,40] where similar phenomenon occurs even at smaller length scales.

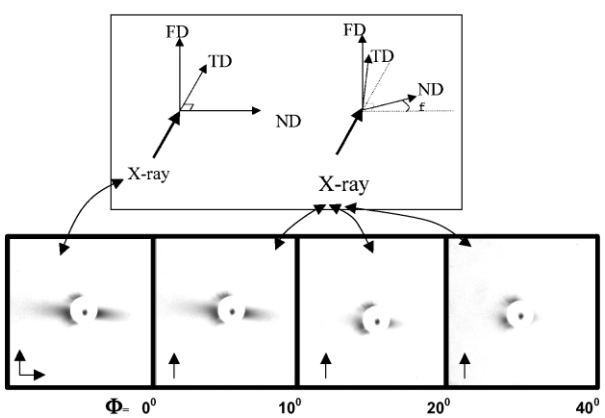

Fig. 17. SAXS patterns of the rotated B-cut samples in the skin region of nylon 6 nanocomposites (30 min exposure). Rotation angles about FD are shown under each pattern.

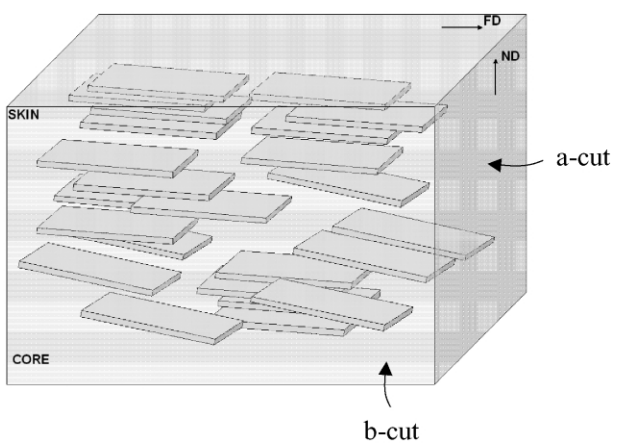

Fig. 18. Schematics of orientation of the nanoplatelets from skin to core of the compounded samples molded at 50 °C.

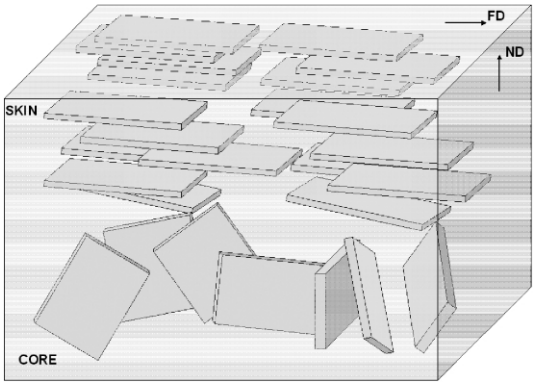

Fig. 19. Schematics of orientation of the nanoplatelets from skin to core of the compounded samples molded at 130 °C.

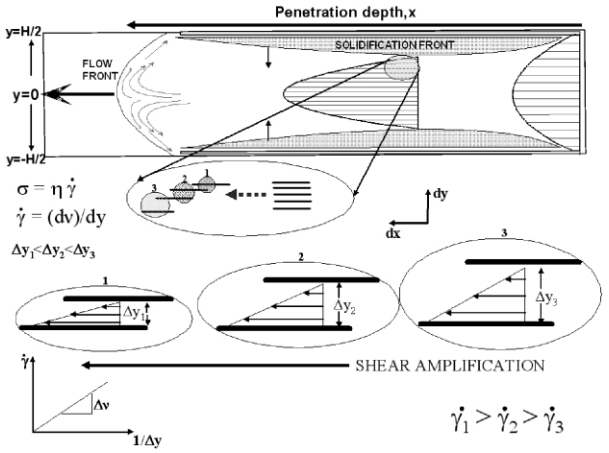

Fig. 21. Shear amplification mechanism.

Appendix A

A.1. Orientation factors

Wilchinsky's geometrical rule for the monoclinic α form resulted in the following relations:

$$\langle \cos^2_{\chi b,z}\rangle = 1 - 1.4717\langle \cos^2 \chi_{200,z}\rangle - 0.8721\langle \cos^2 \chi_{(002,202),z}\rangle \quad \text{(A1.1)}$$

$$\langle \cos^2 \chi_{c,z}\rangle = 1.172\langle \cos^2 \chi_{002,z}\rangle \quad \text{(A1.2)}$$

$$\langle \cos^2 \chi_{a,z}\rangle = 1.4717\langle \cos^2 \chi_{200,z}\rangle - 0.8356\langle \cos^2 \chi_{,202,z}\rangle + 0.5357\langle \cos^2 \chi_{,002,z}\rangle \quad \text{(A1.3)}$$

with

$$f_{b,z} = \tfrac{1}{2}(3\langle \cos^2 \chi_{b,z}\rangle - 1) \quad \text{(A1.4)}$$

$$f_{a,z} = \tfrac{1}{2}(3\langle \cos^2 \chi_{a,z}\rangle - 1) \quad \text{(A1.5)}$$

$$f_{c,z} = \tfrac{1}{2}(3\langle \cos^2 \chi_{c,z}\rangle - 1) \quad \text{(A1.6)}$$

and for the monoclinic γ phase

$$\langle \cos^2 \chi_{c,z}\rangle = 1.3611\langle \cos^2 \chi_{001,z}\rangle \quad \text{(A1.7)}$$

with

$$-f_b = 2f_a = 2f_c \quad \text{(A1.8)}$$

A.2. Shear rate analysis during cavity filling

The coordinate axes are shown in Fig. 21.

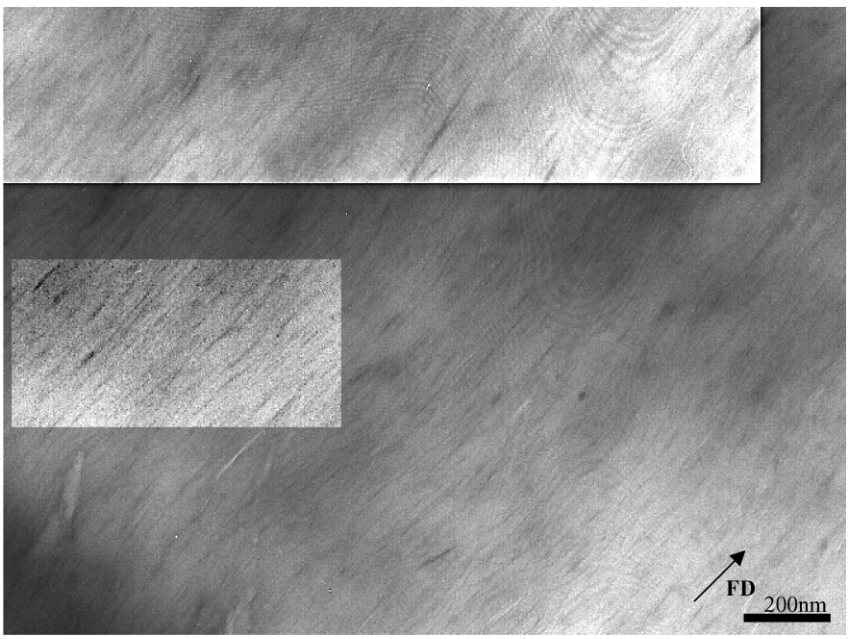

Fig. 20. TEM image of nylon 6 nanocomposite taken close to the surface region (inset selected two regions were image enhanced for clarity).

For unfilled nylon 6

Momentum balance equation

$$\frac{dp}{dx} = -\frac{d\tau_{yx}}{dy} \tag{A2.1}$$

where x: penetration depth of the polymer fluid in the cavity, y: distance in the normal direction (thickness direction), P: pressure, τ_{yx}: shear stress along the thickness direction.

Inserting the above equation into a simple constitutive equation and using boundary conditions at $y = 0$, $\tau_{yx} = 0$ yields

$$\tau_{yx} = \eta\frac{dv_x}{dy} = -\frac{dp}{dx}y \tag{A2.2}$$

where η: Newtonian viscosity of the polymer melt, v : velocity of the fluid along the x directionand finally shear rate is found from

$$\dot{\gamma} = \frac{dv_x}{dy} = -\frac{y}{\eta}\frac{dp}{dx} \tag{A2.3}$$

Since the pressure gradient is constant due to fully developed flow assumption, shear rate can be roughly calculated along the normal direction using the geometry of the part, viscosity of the material and the injection pressure.

$$\dot{\gamma} = -\frac{y}{\eta}\frac{P_0}{X} \tag{A2.4}$$

where

P_0: injection pressure ($650\ \text{Psi} = 4.48 \times 10^6\ \text{Pa}$), X: length of the strip along the x-direction (120 mm), $\eta =$ viscosity (~ 500 Pa. s from viscosity vs. shear rate capillary data).

Then at $y = -H/2 = 1.5$ mm

$$\dot{\gamma} = 170\ \text{s}^{-1} \tag{A2.5}$$

For nanoplatelet filled nylon 6

Momentum balance equation

$$\frac{dP}{dx} = \frac{d\tau_{yx}}{dy} = \eta\frac{d^2v_x}{dy^2} \tag{A2.6}$$

where x: penetration depth of the polymer fluid in the cavity, y: normal direction between two infinite platelets, P: pressure, τ_{yx}: shear stress along the normal direction.

Since the nanoplatelets have very large surface areas and show a continuous arrangement from the gate to the end of the cavity, the effective penetration depth X can be assumed to be equal in the absence and presence of fillers.

Boundary conditions $v_x(H) = 0$, $v_x(0) = v_x$, where H is the distance between the lower and upper nanoplatelet, yields

$$\dot{\gamma} = \frac{dv_x}{dy} = \frac{1}{\eta}\frac{dP}{dx}\left(y - \frac{H}{2}\right) - \frac{v_x}{H} \tag{A2.7}$$

The shear rate varies across the gap distance of the platelets. However, since the value of H and y is in the nanometer range, the first and the second term become negligible and the shear rate can be approximated by the following relationship:

$$\dot{\gamma} \approx \frac{v_x}{H} \tag{A2.8}$$

where H: the distance between the lower upper nanoplatelet (~ 30 nm), v_x: approximate velocity of the plates assumed from injection speed (2.02–17 cm/s).

It is obvious from Eq. (A2.8) that shear rate is amplified greatly due to nano dimension of the denominator term regardless of the velocity term in the numerator.

The range is calculated as

$$\dot{\gamma} \approx 6.7 \times 10^6\ \text{s}^{-1} \text{ to } 6.7 \times 10^5\ \text{s}^{-1} \tag{A2.9}$$

and

$$\frac{\dot{\gamma}_{\text{filled}}}{\dot{\gamma}_{\text{unfilled}}} \approx 4000\ to\ 40,000 \tag{A2.10}$$

Acknowledgement

We would like to thank Dr Kris Akkapeddi of Honeywell who has kindly provided the materials.

References

[1] Nielsen LE. Mechanical properties of polymers and composites. New York: Marcel Dekker; 1974.
[2] Giannelis EP. Advanced Materials 1996;8(1):29–35.
[3] Fujiwara S, Sakamoto T. Japanese Pat. 1976; Jp-A-51-109998.
[4] Usuki A, Kojima Y, Okada M, Kurauchi T, Kamigaito O, Deguchi R. Polym Prepr Jpn 1990;39:2427.
[5] Usuki A, Kojima Y, Kawasumi M, Okada A, Fukushima Y, Kurauchi T, Kamigaito O. J Mater Res 1993;8:1179–83.
[6] Usuki A, Kawasumi M, Kojima Y, Okada A, Kurauchi T, Kamigaito O. J Mater Res 1993;8:1174–8.
[7] Liu LM, Qi ZN, Zhu XG. J Appl Polym Sci 1999;71:1133–8.
[8] Fukushima Y, Okada A, Kawasumi M, Kurauchi T, Kamigaito O. Clay Mineral 1988;23:27–34.
[9] Kojima Y, Usuki A, Kawasumi M, Okada A, Kurauchi T, Kamigaito O. J Polym Sci: Part A 1993;31:983–6.
[10] Kojima Y, Usuki A, Kawasumi M, Okada A, Kurauchi T, Kamigaito O. J Polym Sci: Part A 1993;31:1755–8.
[11] Yasue K, Katahira S, Yoshikawa M, Fujimoto K. Polymer-clay nanocomposites. Pinnavaia TJ, Beall EW, editors. New York: Wiley 2002.
[12] Yang F, Ou Y, Yu Z. J Appl Polym Sci 1998;69:355–61.
[13] Russel PD, Beaumont WRP. J Mater Sci 1980;15:197–207.
[14] Zdenek M, Chompff JA. J Polym Sci: Part B 1974;12:977–89.
[15] Varlot K, Reynaud E, Loppfer MH, Vigier G, Varlet J. J Polym Sci: Part B 2001;39:1360–70.
[16] Keuchel K. MS Thesis, University of Akron, 1994.
[17] Hsiung CM, Cakmak M, White JL. Polym Sci 1990;30(16):967.
[18] Hsiung CM, Cakmak M, White JL. Int Polym Proc 1990;5(2):109.
[19] Ulcer Y, Cakmak M. Polymer 1994;35:5651.
[20] Hsiung C, Cakmak M. J Appl Polym Sci 1993;47:149.
[21] Ulcer Y, Cakmak M, Miao JW, Hsiung CM. J Appl Polym Sci 1996; 60:669.

[22] Wilchinsky ZW. Encyclopedia Polym Sci Tech 1968;9:624–48.
[23] Kyotani M, Mitsuhashi S. J Polym Sci: Part A-2 1972;10:1497–508.
[24] Yalcin B, Cakmak M. Polymer (submitted).
[25] Holmes DR, Bunn CW, Smith DJ. J Polym Sci 1955;17:159.
[26] Kinoshita Y. Makromol Chem 1959;33:1.
[27] Arimoto H. J Polym Sci: Part A 1964;2:2283.
[28] Arimoto H, Ishibash M, Hirai M, Chatani Y. J Polym Sci: Part A 1965; 3:317.
[29] Ueda S, Kimura T. Chem High Polym Jpn 1958;15:243.
[30] Tsuruda M, Arimoto H, Ishibashi M. Chem High Polym Jpn 1958;15: 619.
[31] Vogelsong DC. J Polym Sci: Part A 1963;1:1055.
[32] Miyakasa K, Ishikawa K. J Polym Sci: Part A 1968;2(6):1317.
[33] Bradbury EM, Brown L, Elliot A, Parry DAD. Polymer 1965;6:465.
[34] Keuchel A. PhD Dissertation, University of Akron, 1997.
[35] Isa IA. J Polym Sci, Polym Chem Ed 1971;9:199.
[36] Murthy NS, Szollosi AB, Sibilia JP, Krimm SJ. Polym Sci, Polym Phys Ed 1985;23:2369.
[37] Medellin-Rodriguez FJ, Burger C, Hsiao BS, Chu B, Vaia R, Philips S. Polymer 2001;42:9015–23.
[38] Nagatoshi F, Arakawa T. Polym J 1970;1(6):685–90.
[39] Hsiung CM, Tian J, Cakmak M. Int Polym Process 1993;8(2):164–77.
[40] Hsiung CM, Cakmak M. Int Polym Process 1993;8(3):255–70.